Tuning $MgB_2(0001)$ surface states through surface termination

V. Despoja,[1,2,*] D. J. Mowbray,[1,3] and V. M. Silkin[1,2,4]

[1]*Donostia International Physics Center (DIPC), Paseo de Manuel de Lardizabal 4, E-20018 San Sebastián, Spain*

[2]*Departamento de Física de Materiales and Centro Mixto CSIC-UPV/EHU, Facultad de Ciencias Quimicas, Universidad del País Vasco, Apartado 1072, E-20018 San Sebastián, Spain*

[3]*Nano-Bio Spectroscopy Group and ETSF Scientific Development Centre, Departamento de Física de Materiales, Universidad del País Vasco, Avenida de Tolosa 72, E-20018 San Sebastián, Spain*

[4]*IKERBASQUE, Basque Foundation for Science, E-48011 Bilbao, Spain*

(Received 12 May 2011; revised manuscript received 19 July 2011; published 12 September 2011)

Surface state localization and hybridization on B, Mg, and Li terminated $MgB_2(0001)$ surfaces are studied within density functional theory (DFT). For the B terminated surface we find a low energy B σ_1 surface state, a sp_z surface state, and B σ_2 and σ_3 quantum well states, which are 90% localized in the topmost B layer. Our results demonstrate that by charging the B atomic layer, either by changing the surface termination or through electro-chemical doping, the B σ surface states are shifted down in energy, filled, and delocalize through hybridization as they cross the bulk MgB_2 bulk bands. On the other hand, the sp_z surface state should be shifted up in energy, emptied, and gain an increasingly metallic s character by adding a Mg, Mg^{+1}, or Li terminating atomic layer. These results clearly show both the robust nature of $MgB_2(0001)$ surface states, and how their localization and energy range may be tuned by surface termination and charging, with implications for the superconducting and plasmonic behavior of MgB_2.

DOI: 10.1103/PhysRevB.84.104514 PACS number(s): 73.20.−r, 74.25.Jb, 74.70.Ad

I. INTRODUCTION

Since 2001 when superconductivity in MgB_2 was first discovered,[1] many calculations of its bulk and surface electronic structure have been performed. In general, these calculations showed a good agreement with angle-resolved photoemission spectroscopy (ARPES) experiments, suggesting that MgB_2 is not a strongly correlated system, and that superconductivity is probably a consequence of some strong electron-phonon coupling mechanism. In other words, MgB_2 appears to be an extreme case of an Eliashberg superconductor. Indeed, many studies show strong coupling of σ electrons and e_{2g} phonons in the B layer, and a wide superconducting gap in the σ band has been measured.[2] Also, since the recent fabrication of pristine ultrathin MgB_2 films,[3] surface enhanced superconductivity has become an increasingly active area of research.[3]

These theoretical investigations greatly contributed to the understanding of the peculiar bulk/surface electronic structure of the seemingly simple MgB_2 crystal. Bulk electronic structure calculations[4–7] show that MgB_2 has five main bands, namely completely filled σ_1 B, partially filled σ_2, σ_3, and p_z B, along with completely unoccupied s Mg bands. Bonding within the B layers is mostly covalent (sp^2 hybridization) and ionic/metallic between B–Mg–B layers.

Due to the Mg between the B planes, the nature of in-plane covalent bonding is not typical, as in graphite for example. Specifically, the presence of Mg enhances the interlayer overlap and induces strong hybridization between dangling B p_z and Mg s orbitals (sp_z bond). This causes an upward shift of the Mg s and downward shift of the B p_z band. In other words, this induces an emptying of the Mg s and filling of the B p_z bands. In this way Mg atoms donate electrons interstitially (between B–Mg layers) and become positively ionized. This causes an additional downward shift of the B π band relative to the B σ bands and charge transfer from the σ to the π band.

In this way MgB_2 has a small hole doping of the higher energy σ_2 and σ_3 bands (at the Γ point) and bonds within the B layers become mixed covalent/metallic. Such hole doping in the B layers enhances the superconductivity. This is similar to the case of intercalated graphites,[8] where doping (interplane intercalation) by alkali metals causes the graphite to become superconducting.

The above description is also consistent with charge density distributions calculated in Ref. 4, where it was seen that Mg atoms are strongly ionized, but electrons are donated interstitially, rather than directly to the B layers, and interlayer bonding is much more metallic than ionic. Also, it has been shown that less charge is participating in the in-plane B–B bonding in MgB_2 compared to the C–C bonding in primitive graphite. This suggests that Mg induces a covalent bonding in the B layer which is not completely saturated and is weakened, that is, slightly metallic.

On the other hand, the electronic structure of the MgB_2 surface is much more delicate. Due to the weak dispersion of bulk B σ bands in the (0001) direction, there exist two wide gaps in the projected bulk band structure of MgB_2 at the $\overline{\Gamma}$ point. This allows for the formation of many different types of surface states. Indeed, several studies of the $MgB_2(0001)$ surface[9–12] showed the existence of various surface and subsurface states, whose positions and existence depend on crystal termination and coverage.[13]

For the case of a B terminated surface, every bulk band has its own surface state band which follows the upper edge of the corresponding projected bulk band. All these states are mostly localized in the first few B layers. For example, the surface state band for B terminated MgB_2 reported in Ref. 11 has p_z symmetry and is located on the upper edge of the projected p_z bulk band. Its energy at the $\overline{\Gamma}$ point in the surface Brillouin

zone (SBZ) is about −2.7 eV and its charge density is mostly distributed throughout the first three B layers.

In the case of the Mg terminated surface, there is one surface state whose energy at the $\overline{\Gamma}$ point is about −2 eV. This surface state has sp_z symmetry and is mostly localized above the surface plane in the vacuum region (suprasurface).

However, ARPES measurements which followed[14] showed a good agreement with bulk electronic structure calculations,[5–7] although the peak at 0.5 eV in the normal photoemission does not agree with any of the above mentioned surface states. The calculations of Servedio *et al.*[12] showed good agreement but are not particularly relevant, as the surface potential barrier was there modeled by a step potential, so that the binding energy of the surface state was strongly dependent on the position of the potential step. On the other hand, calculations by Profeta *et al.*[13] showed that the sp_z surface state at the $\overline{\Gamma}$ point strongly depends on the termination and coverage of the MgB_2 crystal, indicating that in the experiment[14] the surface termination may have been mixed or had significant surface contamination. Uchiyama *et al.*[2] paid much more attention to surface preparation, and in their measurement the normal photoemission peak appeared at −1.0 eV. In Refs. 15–17 an 18 monolayer (ML) thick (18 ML B and 18 ML Mg layers) MgB_2 film was deposited an a Mg(0001) substrate using the molecular beam epitaxy (MBE) co-deposition technique. Following this it was determined (using several techniques including XPS, LEED+XRD, x-ray absorption) that indeed there was no surface contamination, and ARPES measurements were then performed. The results showed an excellent agreement of the projected bulk band structure with bulk calculations.[5,6] Agreement with surface band structure calculations[11] was also quite good. For example, peaks at about −1.6 and −3.2 eV are measured which correspond to sp_z surface states in Mg and B terminated surfaces, respectively. Measurements in Refs. 5 and 6 also suggested that the most stable surface termination is Mg, as was anticipated in Refs. 10 and 13.

Recent experimental realizations of the MgB_2 surface have been brought to an increasingly high level of precision.[2,3,15–17] These experiments were aimed at investigating the fine superconductivity properties of MgB_2, for example, multiple superconductivity gaps,[2] and surface enhanced superconductivity.[3] However, such clean MgB_2 surfaces, with a very well defined electronic structure, can also be an excellent starting point for the investigation of both optical and dielectric MgB_2 surface properties. It also should be noted that in Ref. 3 ultrathin MgB_2 films down to 7.5 nm were fabricated, which is quite close to the thicknesses used in the calculations shown herein.

Interplay between 2D and 3D electronic structures give rise to the unique dielectric[18–22] and extraordinary optical properties[23–25] of the MgB_2 crystal. On the other hand, because of the plethora of surface, localized and subsurface states, the MgB_2 surface dielectric and optical properties may be even more interesting. Before providing such theoretical calculations we require an accurate description of the surface electronic structure.

For this reason, we will focus here on the investigation of three (B, Mg, and Li) terminated MgB_2 surface electronic structures by comparing the results of three different (two plane wave and one real space) *ab initio* density functional theory (DFT) methods. In so doing, we may demonstrate how by changing the surface termination, charging, and doping the $MgB_2(0001)$ surface we may tune both the localization and energy range of the surface and subsurface states, with potential applications in the areas of plasmonics and superconductivity.

The paper is organized as follows. In Sec. II we describe the *ab initio* methods used for the surface electronic structure calculations, the description of surface formation energies, and develop criteria to distinguish between surface, subsurface, vacuum, and bulk states. The numerical results are presented in Sec. III for B, Mg, and Li terminated surfaces, with results for each termination in separate subsections. These results are then discussed in more detail in Sec. V, where we show how surface termination and electrochemical doping may be used to tune $MgB_2(0001)$ surface states. This is followed by a concluding section.

II. METHODOLOGY

Structural optimization and electronic structure calculations for each $MgB_2(0001)$ surface have been performed by combining three different *ab initio* codes. Specifically, we compare our own pseudopotential based plane wave DFT code (SPPW) and the plane wave self-consistent field DFT code (PWscf) belonging to the quantum espresso (QE) package,[26] with a real-space projector augmented wave function method DFT code (GPAW).[27,28]

In each case we have employed the Perdew-Zunger local density approximation (LDA) for the exchange correlation (xc) potential.[29] An electronic temperature of $k_BT \approx 0.1$ eV was used to converge the Kohn-Sham wave functions, with all energies extrapolated to 0 K. The electronic density was calculated using a $12 \times 12 \times 1$ Monkhorst-Pack special k-point mesh, that is, by using 19 special points in the irreducible part of the SBZ.

In both SPPW and PWscf, LDA based pseudopotentials for Li, Mg, and B were used,[30] and the energy spectrum was found to be converged with a 25 Ry plane wave cutoff. For GPAW we employed a grid spacing $h \approx 0.25$ Å in the $MgB_2(0001)$ surface plane, and $h \approx 0.20$ Å normal to the surface, which yielded converged results.

As initial atomic coordinates we consider the system to be a hexagonal lattice with lattice parameters a and c taken from the bulk experimental values, $a \approx 5.8317$ a.u. ≈ 3.086 Å and $c \approx 6.6216$ a.u. ≈ 3.504 Å from Ref. 1, which were previously shown to change by less than 0.6% upon structural optimization of the MgB_2 bulk.[10] Structural optimization is performed within QE,[26] and the system is structurally optimized until a maximum force below 0.001 Ry/a.u. ≈ 0.026 eV/Å was obtained.

Schematics of the relaxed $MgB_2(0001)$ surface supercell models with B, Mg, and Li termination are shown in Fig. 1. The B terminated surface was modeled using a supercell consisting of 9 Mg and 10 B alternating layers, while the Mg terminated surface was obtained by adding Mg layers on top of each surface, with the Li terminated surface formed by replacing the two Mg surface layers with two Li layers. For all terminations four unit cells of vacuum, that is, $4c \approx 26.4864$ a.u. ≈ 14.016 Å, were used to separate the surfaces. This was found

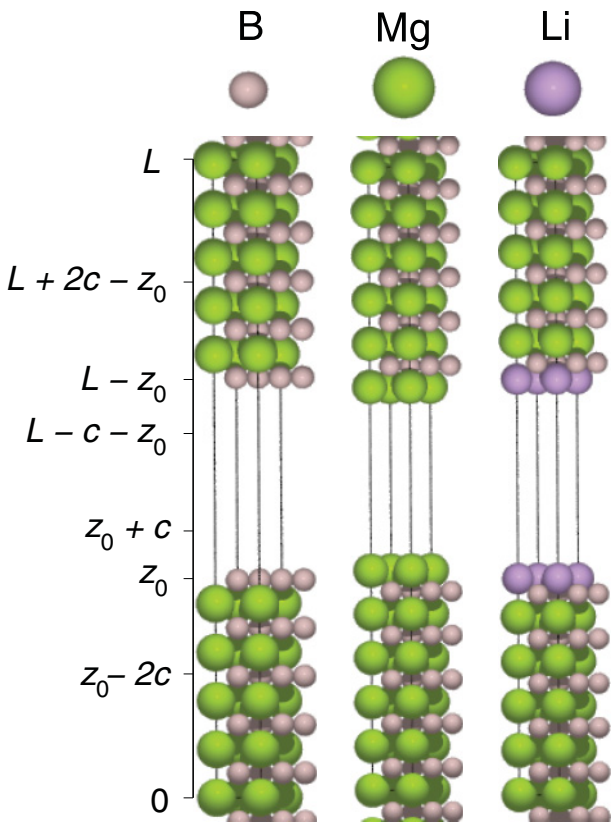

FIG. 1. (Color online) Schematic of the structurally optimized MgB_2(0001) surface unit cells with B, Mg, and Li termination, repeated twice in each direction.

to be sufficient to ensure a good description of both surface and bulk states.

To estimate the relative stability of the B, Mg, and Li terminated MgB_2(0001) surfaces, we consider the surface formation energy ΔE_f, which is defined as the total energy difference from the bulk, and the chemical potential for each of the terminating species, per unit area of the surface.[32] More precisely,

$$\Delta E_f \equiv \frac{E_{\text{Slab}} - N_f E_{\text{Bulk}} - \sum_{\text{X}} c_{\text{X}} \mu_{\text{X}}}{2\mathcal{A}}, \qquad (1)$$

where E_{Slab} is the total energy of the slab, $\mathcal{A} \approx 29.4524$ a.u. ≈ 8.2475 Å ^{2} is the surface area of the unit cell, N_f is the number of MgB_2 bulk layers per unit cell, c_{X} is the number of atoms added or removed from the slab to obtain a given surface termination and μ_{X} is the chemical potential for species X $\in$ {B,Mg,Li}, as taken from Ref. 31. Values for all parameters are provided in Table I.

To differentiate between surface states, vacuum states, subsurface states, and bulk states, we first consider the wave function's projected density in the z direction normal to the surface $\varrho_{n,\mathbf{k}}(z)$. This is defined as

$$\varrho_{n,\mathbf{k}}(z) \equiv \iint_{\mathcal{S}} |\psi_{n,\mathbf{k}}(x,y,z)|^2 dx dy, \qquad (2)$$

where $\{x,y\}$ are surface coordinates, $\mathcal{S}$ is the surface area of the unit cell, and $\psi_{n,\mathbf{k}}$ is the nth Kohn- Sham wave function at k-point $\mathbf{k}$. We then apply the criterion that the wave function's weight on the surface, $s_{n,\mathbf{k}}$, surpasses a certain threshold, where

TABLE I. GPAW calculated formation energies ΔE_f for B, Mg, and Li terminated MgB_2(0001) surface in eV/Å^2 and J/m^2 relative to bulk MgB_2 and the chemical potential of the terminating metal in the bulk for species X, μ_{X}, taken from Ref. 31.

MgB_2(0001)	B terminated	Mg terminated	Li terminated
E_{Slab} (eV)	−164.31	−170.45	−171.92
E_{Bulk} (eV)	−16.95	−16.95	−16.95
N_f	9	10	10
μ_{X} (eV/atom)	5.81	1.51	1.63
$c_{\text{B}}, c_{\text{Mg}}, c_{\text{Li}}$	1, 0, 0	0, 1, 0	0, −1, 2
ΔE_f (eV/Å^2)	−0.01	0.03	−0.04
ΔE_f (J/m^2)	−0.12	0.56	−0.63

we define the surface region as two bulk unit cells below the surface layer, and one unit cell of vacuum above the surface layer. In more detail, we define

$$s_{n,\mathbf{k}} = \int_{z_0-2c}^{z_0+c} \varrho_{n,\mathbf{k}}(z)dz + \int_{L-z_0-c}^{L-z_0+2c} \varrho_{n,\mathbf{k}}(z)dz, \qquad (3)$$

where z_0 is the surface layer coordinate and L is the length of the unit cell in the z direction, as depicted in Fig. 1. States which have more than two thirds of their weight in the surface region, that is, $s_{n,\mathbf{k}} \gtrsim 0.66$, are then considered to be surface states.

In order to further distinguish between subsurface states which penetrate deep into the crystal, surface resonant states, and bulk states, we increased the thickness of the supercell, by adding six bulk unit cells in the center of the slab. The resulting structure was then relaxed within QE employing a coarser k-point mesh of $8 \times 8 \times 1$, to obtain the ground-state geometry.

To understand how surface states disperse through the SBZ and hybridize with bulk states, we consider the overlap integrals between the Kohn-Sham wave functions at neighboring k points, separated by $\Delta\mathbf{k}$. In real space this is defined simply as

$$\langle \psi_{n,\mathbf{k}} | \psi_{n',\mathbf{k}+\Delta\mathbf{k}} \rangle_{\mathcal{V}} = \int_{\mathcal{V}} \psi^*_{n,\mathbf{k}}(\mathbf{r}) \psi_{n',\mathbf{k}+\Delta\mathbf{k}}(\mathbf{r}) d\mathbf{r}, \qquad (4)$$

where $\mathbf{r} = \{x,y,z\}$ is the real-space coordinate, and $\mathcal{V}$ is the volume of the unit cell. Then $\psi_{n,\mathbf{k}} \to \psi_{n',\mathbf{k}+\Delta\mathbf{k}}$ for n' which maximizes $|\langle \psi_{n,\mathbf{k}} | \psi_{n',\mathbf{k}+\Delta\mathbf{k}} \rangle_{\mathcal{V}}|$. In this way we may distinguish between band crossings and avoided crossings in the band structure, and trace the surface states throughout the SBZ.

III. RESULTS

The DFT estimates of the surface formation energy ΔE_f shown in Table I are quite small ($|\Delta E_f| \lesssim 0.05$ eV/Å^2), which suggests that each of the MgB_2(0001) surface terminations considered should be stable experimentally. This is clear when one compares with the much higher surface formation energies obtained for other materials, such as metal oxides, which are known to be stable experimentally.[32] In particular, we find it should be thermodynamically preferred to replace a Mg surface termination by a Li termination, so that surface doping by Li is quite feasible. It should be noted that our choice of bulk metallic B, Mg, and Li for the chemical potentials

shown in Table I has a significant influence on the resulting formation energies obtained. However, the main conclusion that each surface termination should be obtainable under particular experimental conditions should still hold.

The projection of the bulk band structure in a direction perpendicular to the crystal surface ($\Gamma \rightarrow$ A) is a fingerprint of the particular crystal structure. The same is true for a $MgB_2(0001)$ surface, for which the projected band structure is actually quite simple. Due to the weak B–B layer overlap, there are three rather narrow B σ bands (σ_1, σ_2, and σ_3), while the overlap between p_z orbitals in the B layers and s orbitals in Mg layers yields a wider π band. The π band is then separated from σ bands by two wide gaps, which are noticeable in Figs. 3, 6, and 9.

Since the surface band structure of B and Mg terminated $MgB_2(0001)$ surfaces was previously studied in Refs. 11 and 13, we will focus here on the detailed classification of the surface and subsurface states and surface state resonances in Mg, B, and Li terminated $MgB_2(0001)$. This is accomplished by combining both pseudopotential-based plane wave methods (SPPW, PWScf) and a real space projector augmented wave function method (GPAW) to test the robustness of the surface states, and geometry optimization to show how surface relaxation can modify them.

A. B-terminated $MgB_2(0001)$ surface

To understand how movement of the atomic planes in the surface region influences the energy and character of the surface and subsurface states, the B terminated surface electronic structure has been calculated both with and without structural optimization. The relative changes in the (B–Mg) interlayer separation compared to the bulk values Δ_{ij} are provided in Table II.

We find that the relative change in the interlayer separation is quite small, in agreement with previous plane wave calculations[10] using the PBE xc functional[33] where only the top four atomic layers were relaxed. This rigidity of the structure is reflected in the band structure calculations shown in Fig. 3. We find that the band structures with and without structural optimization do not differ significantly for the B terminated surface.

TABLE II. Change in B terminated Mg–B interlayer separation $\Delta_{i,j}$ between the ith and jth layers from the surface, relative to the bulk MgB_2 experimental geometry.

	PWscf LDA[a]		VASP PBE[b]	
$\Delta_{0,1}$[B–Mg]	−4.4%	−7.8 pm	−2.1%	−3.7 pm
$\Delta_{1,2}$[Mg–B]	0.4%	0.75 pm	2.0%	3.5 pm
$\Delta_{2,3}$[B–Mg]	−1.1%	−2.0 pm	0.9%	1.6 pm
$\Delta_{3,4}$[Mg–B]	−1.7%	−3.1 pm	−1.8%	−3.2 pm
$\Delta_{4,5}$[B–Mg]	−1.3%	−2.6 pm	0%	0.0 pm
$\Delta_{5,6}$[Mg–B]	−1.3%	−2.3 pm	—	—
$\Delta_{6,7}$[B–Mg]	−1.5%	−2.7 pm	—	—
$\Delta_{7,8}$[Mg–B]	−1.3%	−2.3 pm	—	—
$\Delta_{8,9}$[B–Mg]	−0.75%	−1.4 pm	—	—

[a]This work.
[b]Ref. 10.

The energies of the surface and subsurface states at the $\overline{\Gamma}$, $\overline{\mathrm{K}}$, and $\overline{\mathrm{M}}$ points for the structurally unoptimized and optimized surfaces are also shown in Fig. 3. We find that the B terminated surface has several surface and subsurface states, consisting of three localized bands which are well separated from their corresponding bulk bands. For these localized bands we plot $\varrho_{n,\mathbf{k}}$ in Fig. 2 at $\overline{\Gamma}$, $\overline{\mathrm{K}}$, and $\overline{\mathrm{M}}$ points. The deepest subsurface state's band [Figs. 2(a)–2(c)] consists of B σ_1 orbitals, and is localized mainly in the first and slightly in the second B layer. Specifically, we find for this band $s_{n,\mathbf{k}} \gtrsim 0.66$ throughout the SBZ, as shown in Fig. 4. In fact, the B σ_1 surface band may be described semiquantitatively by a +0.6 eV shift of the top of the B σ_1 bulk bands.

To differentiate between localized states, surface resonances, and bulk states, we recalculated the electronic structure for a thicker slab with six additional MgB_2 bulk layers. These results are shown as insets in the upper right corners of the $\varrho_{n,\mathbf{k}}(z)$ plots in Fig. 2. For the larger slab we clearly see in Fig. 2(b) that the B σ_1 state is indeed a surface state localized on the topmost B atomic layer.

The second group of surface states [Figs. 2(d), 2(h), and 2(j)] are a combination of Mg s and B p_z orbitals. These sp_z surface states are mainly localized above the surface and between B and Mg layers. Figure 4 shows that the sp_z surface state is clearly recognizable as it disperses through the SBZ, although some hybridization occurs when crossing the narrow B $\sigma_{2,3}$ band. As with the B σ_1 band, the sp_z surface band is well described by a +0.6 eV shift of the top of the respective bulk band, in this case the π bands. We also find for B termination the sp_z states decay slowly into bulk, which is also seen for the extended slab shown as insets in Figs. 2(d), 2(h), and 2(j).

The third group of surface states [Figs. 2(g), 2(e), and 2(i)] are B σ states which are more than 90% localized in the topmost B layer. From Fig. 4 we see that the B $\sigma_{2,3}$ surface states may be clearly traced throughout the SBZ, at about 0.6 eV above their respective B $\sigma_{2,3}$ bulk bands. Thus, Fig. 4 shows that for the B terminated $MgB_2(0001)$ surface the B σ_1, sp_z, and B $\sigma_{2,3}$ surface bands are near quantitatively described by rigidly shifting the top of the respective bulk bands up in energy by 0.6 eV.

B. Mg-terminated $MgB_2(0001)$ surface

Even though optimization of the crystal structure only slightly modified the Mg terminated surface (cf. Table III) and band structure (cf. Fig. 6), modifications of the surface electronic structure are quite radical. Density distributions in Fig. 5 show that for the unrelaxed surface there exist two types of localized states, an sp_z surface state [Fig. 5(a)] and B σ subsurface states [Figs. 5(d) and 5(e)]. On the other hand, even though the relaxed surface is only slightly compressed (maximally −2.7% in the first layer), it induces the appearance of new surface states [Figs. 5(b) and 5(c)]. Such states consist of B σ states, which are localized around B layers but penetrate quite deep inside the crystal. At the $\overline{\mathrm{K}}$ point this state may even be considered a surface state resonance. Figure 7 clearly shows that these states are more properly associated with the B σ_2 and σ_3 surface states [Figs. 5(d) and 5(e)].

Another consequence of the surface relaxation is that the B σ surface states [Figs. 5(d), 5(b), and 5(e)] are pushed upward

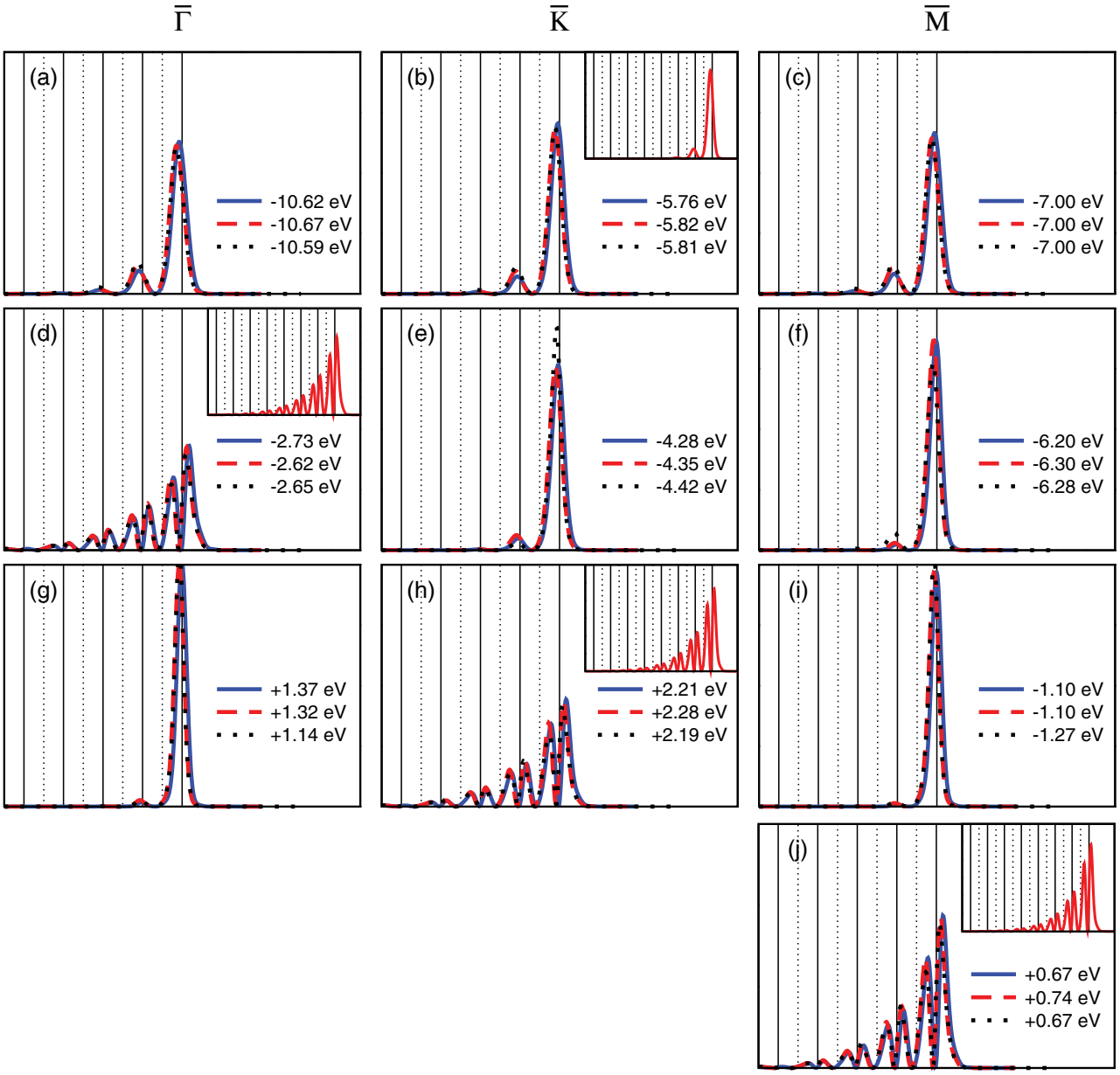

FIG. 2. (Color online) Projected density of surface and subsurface states $\varrho_{n,\mathbf{k}}(z)$ in the B terminated $MgB_2(0001)$ surface vs position normal to the surface plane z, and Kohn-Sham eigenenergies $\varepsilon_{n,\mathbf{k}}$ relative to the Fermi level ε_F. Results from plane wave PWscf calculations before (—) and after (– –) structural optimization are compared with real-space GPAW calculations for the relaxed structure ($\cdots$). Solid and dotted vertical lines denote positions of the B and Mg atomic layers, respectively. Inserts show $\varrho_{n,\mathbf{k}}(z)$ from plane wave PWscf calculations for a relaxed extended supercell model with six bulk unit cells added in the center of the slab.

toward the surface B layers. In other words, in the relaxed crystal the σ surface states are completely localized in the one or two topmost B layers. As shown in Fig. 7, the three B σ bands have definite surface character throughout the SBZ, where they follow the bottom edge of the B σ bulk bands.

We also find relaxation lowers the energy of the σ subsurface states by approximately 0.1 eV at the $\overline{\Gamma}$ and $\overline{\mathrm{K}}$ points, and increases the energy of the sp_z surface state from -1.86 to -1.78 eV at the $\overline{\Gamma}$ point, in better agreement with the experimental value of -1.6 eV. It should also be noted that the B σ_3 surface band is more localized on the topmost B layer in the real-space GPAW calculation. This is attributable to the inherit difficulties plane wave based methods have in describing state localization, compared to real-space methods.

In fact, from Fig. 7 we see that the bottom of all three B σ bands have $s_{n\mathbf{k}} \gtrsim 0.66$ throughout the SBZ. This suggests that adding a layer of Mg shifts the B σ surface bands down in energy by about 0.9 eV relative to the B terminated $MgB_2(0001)$ surface. On the other hand, we find that the sp_z surface band is higher up in energy by about 0.9 eV relative to the B terminated surface. In Sec. IV we will discuss how this rigid shifting in energy of the surface bands may be understood in terms of charging of the $MgB_2(0001)$ surface.

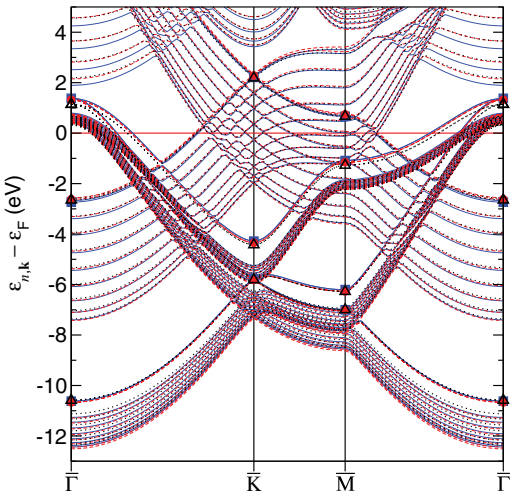

FIG. 3. (Color online) Band structure (lines) and energies of the surface and subsurface states shown in Fig. 2 (symbols) for the B terminated $MgB_2(0001)$ surface in eV relative to the Fermi level ε_F. Results from plane wave PWscf calculations before (— ; ■) and after (– – ; ●) structural optimization are compared with real-space GPAW calculations for the relaxed structure (· · · ; △).

C. Li-terminated $MgB_2(0001)$ surface

To understand how surface charging, or electrochemical doping might affect $MgB_2(0001)$ surface states, we have directly replaced Mg by Li in the first atomic layer (Mg→Li). In effect, this approximates the removal of one electron from each of the Mg terminated surfaces. In other words, replacing Mg by Li resembles a positively charged Mg terminated (Mg^{+1}) surface. This allows us to directly probe the effect of surface charging of the Mg terminated surface without the need for compensating background charges in the calculation. We have then performed structural optimization of the Li terminated $MgB_2(0001)$ surface to model how Li termination

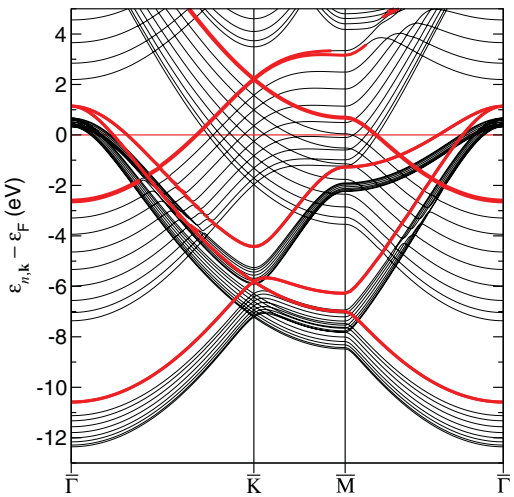

FIG. 4. (Color online) GPAW overlap-based band structure of relaxed B terminated $MgB_2(0001)$ surface, with $\psi_{n,\mathbf{k}} \rightarrow \psi_{n',\mathbf{k}+\Delta\mathbf{k}}$ for n' which maximize $|\langle\psi_{n,\mathbf{k}}|\psi_{n',\mathbf{k}+\Delta\mathbf{k}}\rangle_{\mathcal{V}}|$. Surface states with more than two thirds of their weight in the first vacuum and first two bulk layers, $s_{n,\mathbf{k}} \gtrsim 0.66$, are shown separately as thicker lines.

TABLE III. Change in Mg terminated Mg–B interlayer separation $\Delta_{i,j}$ between the ith and jth layers from the surface, relative to the bulk MgB_2 experimental geometry.

	PWscf LDA[a]		VASP PBE[b]	
$\Delta_{0,1}$[Mg–B]	−5.2%	−9.2 pm	−3.7%	−6.5 pm
$\Delta_{1,2}$[B–Mg]	−0.3%	−0.5 pm	1.2%	2.1 pm
$\Delta_{2,3}$[Mg–B]	−1.9%	−3.3 pm	0.2%	0.4 pm
$\Delta_{3,4}$[B–Mg]	−0.7%	−1.2 pm	0.5%	0.9 pm
$\Delta_{4,5}$[Mg–B]	−0.4%	−0.7 pm	−0.3%	−0.5 pm
$\Delta_{5,6}$[B–Mg]	−0.9%	−1.6 pm	—	—
$\Delta_{6,7}$[Mg–B]	−0.75%	−1.3 pm	—	—
$\Delta_{7,8}$[B–Mg]	−0.9%	−1.6 pm	—	—
$\Delta_{8,9}$[Mg–B]	−0.9%	−1.6 pm	—	—
$\Delta_{9,10}$[B–Mg]	−0.9%	−1.5 pm	—	—

[a]This work.
[b]Ref. 10.

changes the surface states. From Table IV we see that the smaller atomic radius of Li induces a substantial relaxation, with the relaxed Li atomic layer moved down by 52.4 pm towards the B atomic layer.

Both the surface charging and the crystal structure modification strongly change the electronic structure of the surface states. Figure 9 shows that the lowest B σ_1 surface resonance band for the structurally unoptimized surface (Mg→Li ∼ Mg^{+1}), is slightly separated from the upper edge of the bulk B σ_1 band. The density distributions of such states are shown in Figs. 8(a)–8(c) and 8(f), where we see that B σ_1 surface resonances are mainly localized in the four topmost B layers. Structural optimization causes a slight downward shift of the surface resonance B σ_1 bands and induces a strong interaction/hybridization with the bulk B σ_1 band, so that they decay into the bulk states. That is, it increases the amplitude of the propagation of the resonance state into the bulk, as can be seen at the $\overline{\Gamma}$ point in Fig. 8(a). For $\overline{\mathrm{K}}$ and $\overline{\mathrm{M}}$ points, the B σ_1 surface resonances cannot even be distinguished from the normal bulk states and are not shown. This is seen clearly in Fig. 10, with the relaxed Li terminated B σ_1 surface states becoming increasingly bulk-like between $\overline{\Gamma}$ and K, until $s_{n,\mathbf{k}} < 0.66$.

Relaxation also causes a 0.4 eV reduction of the binding energy of the sp_z suprasurface state band. This is expected because relaxation causes contraction of the topmost Li-B interstitial region (cf. Table IV) where the sp_z surface state is mostly located (cf. Fig. 8). The binding energy of the sp_z surface state at the $\overline{\Gamma}$ point is strongly reduced, from about 2.6 to 0.1 eV, comparing with the B terminated surface. This suggests that the binding energy of the sp_z surface state at the $\overline{\Gamma}$ point may be strongly influenced by surface contamination or doping of the B terminated surface, as we will discuss in Sec. IV.

We also find the more localized B σ_2 and σ_3 bands are strongly modified by Li termination. As can be seen in Fig. 9 for Mg→Li∼Mg^{+1}, the B σ_2 and σ_3 surface bands are always slightly separated from the upper edge of the bulk B σ_2 and σ_3 bands, with their density highly localized in the first one or two B layers, as seen in Figs. 8(g), 8(e), and 8(h). These states resemble the highly localized B σ_2 and σ_3 surface states

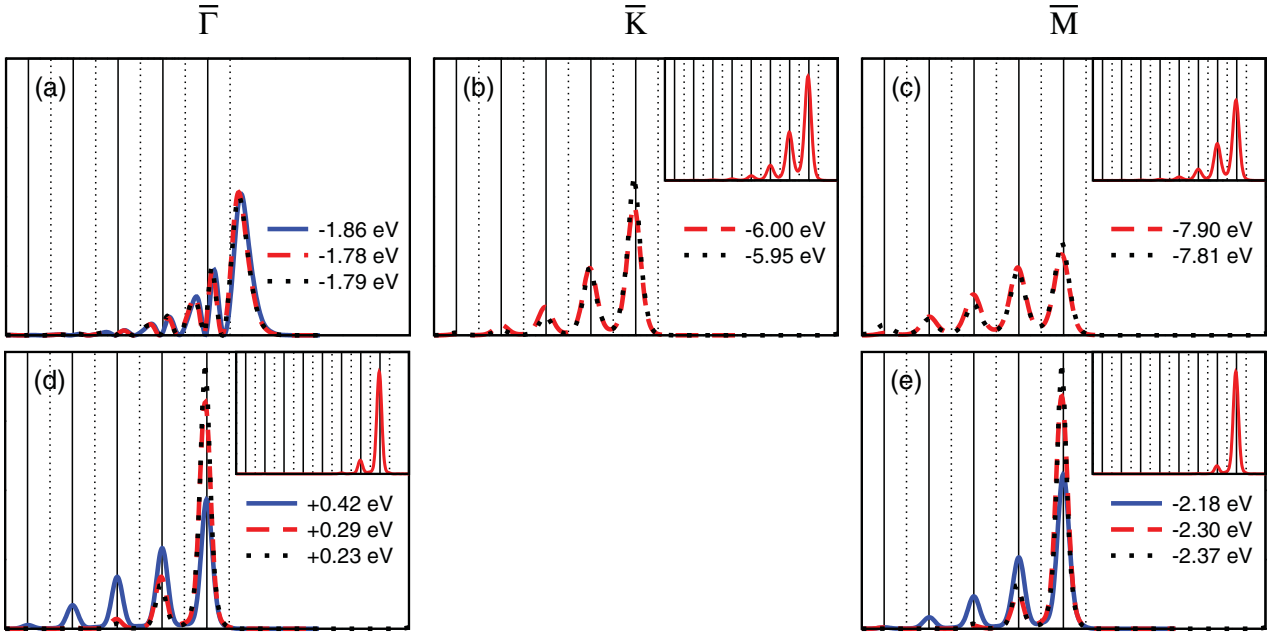

FIG. 5. (Color online) Projected density of surface and subsurface states $\varrho_{n,\mathbf{k}}(z)$ in the Mg terminated $MgB_2(0001)$ surface vs position normal to the surface plane z, and Kohn-Sham eigenenergies $\varepsilon_{n,\mathbf{k}}$ relative to the Fermi level ε_F. Results from plane wave PWscf calculations before (—) and after (– –) structural optimization are compared with real-space GPAW calculations for the relaxed structure (· · ·). Solid and dotted vertical lines denote positions of the B and Mg atomic layers, respectively. Inserts show $\varrho_{n,\mathbf{k}}(z)$ from plane wave PWscf calculations for a structurally optimized extended supercell model with six bulk unit cells added in the center of the slab.

in the B terminated surface. However, surface relaxation shifts the localized B σ_2 and σ_3 bands down in energy. This causes a strong interaction between localized and bulk σ states, with the surface state decaying into the bulk states. This is clearly illustrated by the densities of these states for the relaxed Li terminated structure shown in Figs. 8(e) and 8(h). Here we see that the σ localized state now penetrates substantially into the crystal. By plotting the same distributions for an extended crystal structure [cf. insets of Figs. 8(e) and 8(h)] we see that these states are actually localized state resonances or even pure bulk states at the $\bar{K}$ point. From Fig. 10 we see that the B σ_2 and σ_3 surface states strongly hybridize with the bulk σ states, with $s_{n,\mathbf{k}} < 0.66$ over much of the SBZ.

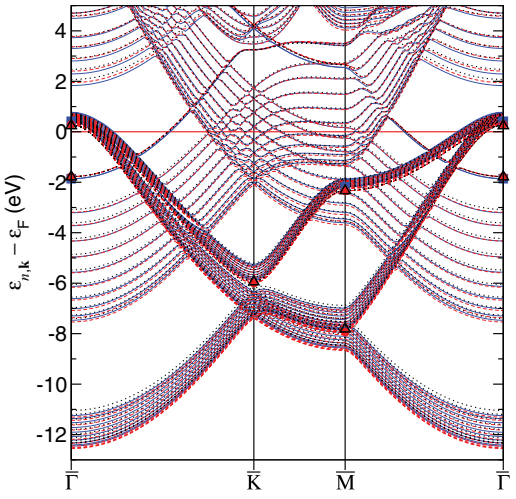

FIG. 6. (Color online) Band structure (lines) and energies of the surface and subsurface states shown in Fig. 5 (symbols) for the Mg terminated $MgB_2(0001)$ surface in eV relative to the Fermi level ε_F. Results from plane wave PWscf calculations before (– ; ■) and after (– – ; ●) structural optimization are compared with real-space GPAW calculations for the relaxed structure (· · · ; △).

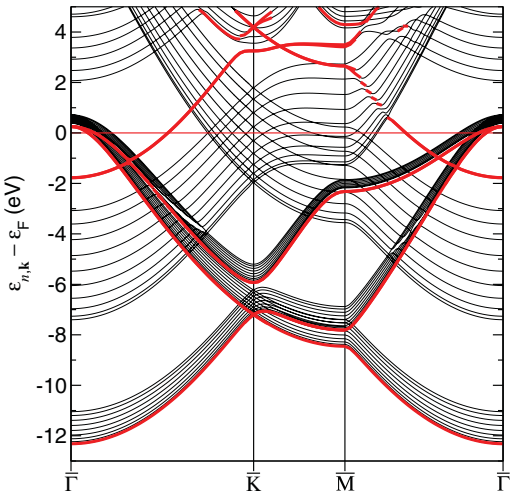

FIG. 7. (Color online) GPAW overlap-based band structure of relaxed Mg terminated $MgB_2(0001)$ surface, with $\psi_{n,\mathbf{k}} \rightarrow \psi_{n',\mathbf{k}+\Delta\mathbf{k}}$ for n' which maximizes $|\langle\psi_{n,\mathbf{k}}|\psi_{n',\mathbf{k}+\Delta\mathbf{k}}\rangle_\nu|$. Surface states with more than two thirds of their weight in the first vacuum and first two bulk layers, $s_{n,\mathbf{k}} \gtrsim 0.66$, are shown separately as thicker lines.

TABLE IV. Change in Li terminated Mg–B interlayer separation $\Delta_{i,j}$ between the ith and jth layers from the surface, relative to the bulk MgB_2 experimental geometry.

		PWscf LDA[a]
$\Delta_{0,1}$[Li–B]	−29.8%	−52.4 pm
$\Delta_{1,2}$[B–Mg]	−0.6%	−1.0 pm
$\Delta_{2,3}$[Mg–B]	−1.2%	−2.2 pm
$\Delta_{3,4}$[B–Mg]	−1.5%	−2.7 pm
$\Delta_{4,5}$[Mg–B]	−1.2%	−2.1 pm
$\Delta_{5,6}$[B–Mg]	−1.5%	−2.6 pm
$\Delta_{6,7}$[Mg–B]	−1.4%	−2.4 pm
$\Delta_{7,8}$[B–Mg]	−1.9%	−3.3 pm
$\Delta_{8,9}$[Mg–B]	−1.5%	−2.6 pm
$\Delta_{9,10}$[B–Mg]	−1.5%	−2.7 pm

[a]This work.

From this we make two observations. First, removing charge from the Mg terminated surface would strongly affect the surface and subsurface states. Second, for the relaxed Li terminated surface all subsurface states hybridize into localized state resonances or bulk states, while the sp_z surface state survives. We will discuss how these affects may be understood and controlled, with the goal of tailoring the surface states of MgB_2, in the following section.

IV. DISCUSSION

Comparing the relative positions of the B σ and sp_z surface states for B, Mg, and Li terminations, shown in Figs. 4, 7, and 10, respectively, clear trends emerge. These suggest that changing surface termination or doping electrochemically can tune both the energy and localization of the $MgB_2(0001)$ surface states.

To demonstrate this point, we replot in Fig. 11 the energies of the surface and subsurface states at the $\overline{\Gamma}$ point as a function of surface termination. As we move from left to right in Fig. 11, charge is transferred to the B atomic layer, as we move from neutral (B), to charging of less than $-1e$ ($Mg \rightarrow Li \sim Mg^{+1}$), of about $-1e$ (Li), and finally, of about $-2e$ (Mg). As charge is donated to the B atomic layer, both the degenerate B σ_2 and σ_3 levels [shown in Fig. 11(a)] and B σ_1 levels [shown in Fig. 11(c)] are filled and move down in energy relative to the bulk MgB_2 Fermi level, in a quasilinear

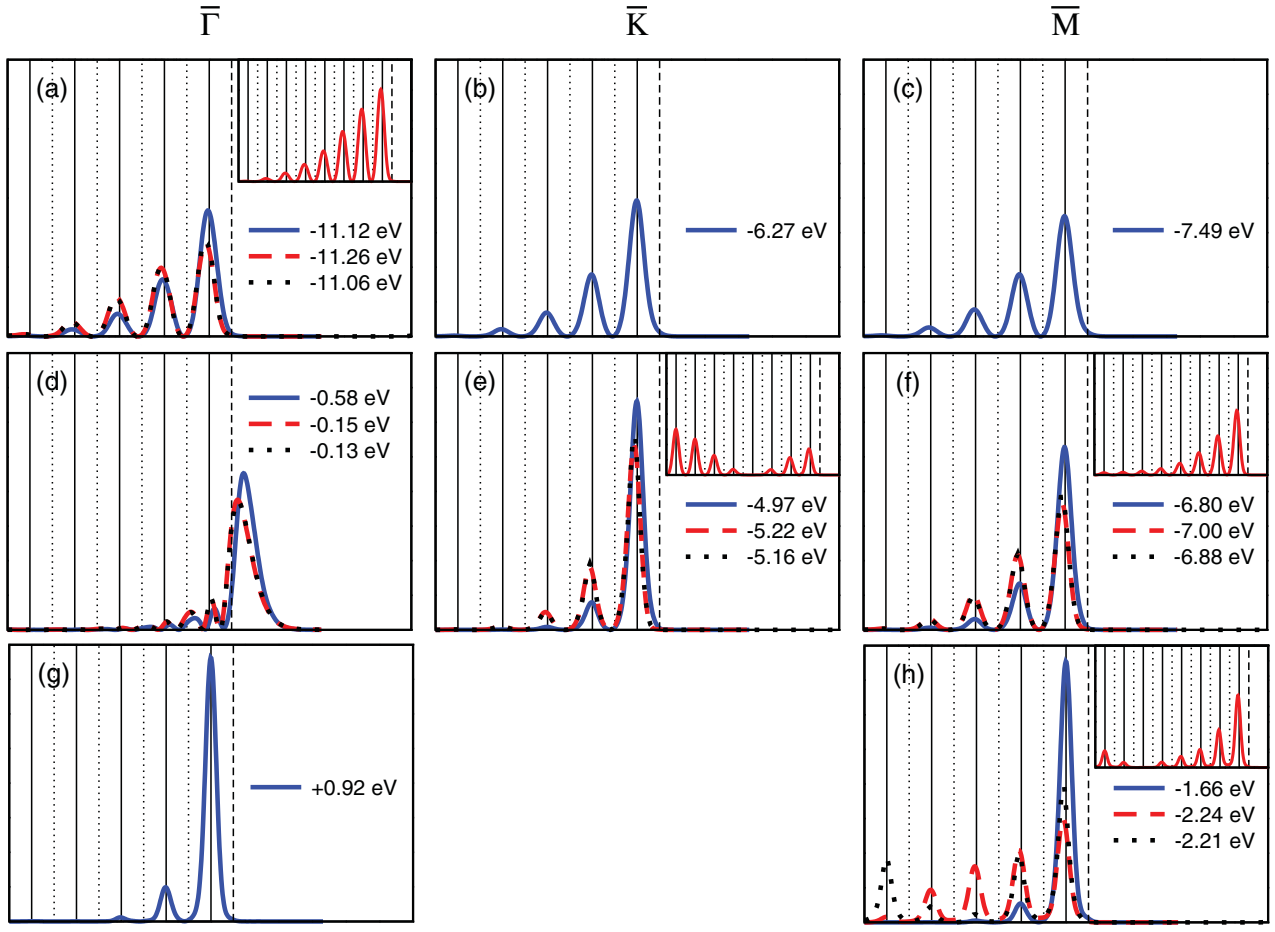

FIG. 8. (Color online) Projected density of surface and subsurface states $\varrho_{n,\mathbf{k}}(z)$ in the Li terminated $MgB_2(0001)$ surface vs position normal to the surface plane z, and Kohn-Sham eigenenergies $\varepsilon_{n,\mathbf{k}}$ relative to the Fermi level ε_F. Results from plane wave PWscf calculations before (—) and after (– –) structural optimization are compared with real-space GPAW calculations for the relaxed structure (· · ·). Solid, dotted, and dashed vertical lines denote positions of the B, Mg, and Li atomic layers, respectively. Insets show $\varrho_{n,\mathbf{k}}(z)$ from plane wave PWscf calculations for a structurally optimized extended supercell model with six bulk unit cells added in the center of the slab.

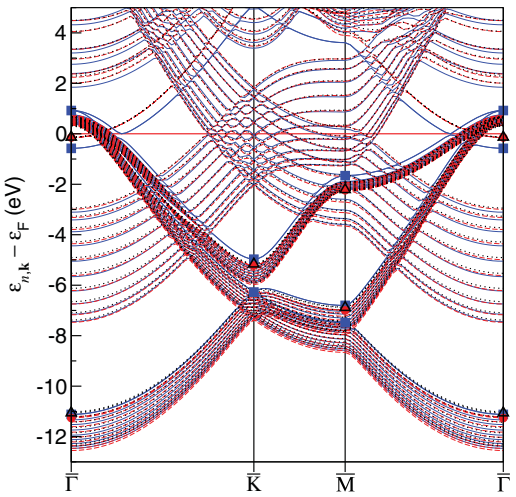

FIG. 9. (Color online) Band structure (lines) and energies of the surface and subsurface states shown in Fig. 8 (symbols) for the Li terminated $MgB_2(0001)$ surface in eV relative to the Fermi level ε_F. Results from plane wave PWscf calculations before (– ; ■) and after (– – ; ●) structural optimization are compared with real-space GPAW calculations for the relaxed structure (· · · ; △).

fashion. Furthermore, when surface states cross the bulk B σ bands, they hybridize, and lose much of their weight on the surface. This is clearly seen in Fig. 10, where for the B σ_2 and σ_3 states $s_{n,\bar{\Gamma}} < 0.66$, and the B σ_1 state shown in Fig. 8(a), also has more weight in the bulk. This strongly suggests that by electrochemically doping the surface, we may tune both the energy and localization of the B σ surface states.

For the higher energy B σ_2 and σ_3 surface states this is particularly interesting, as they resemble quantum well (QW) states. This is because the occupying electrons effectively feel the potential of a QW centered around the B layer. Moreover, electrons in such states are trapped in the topmost B layer

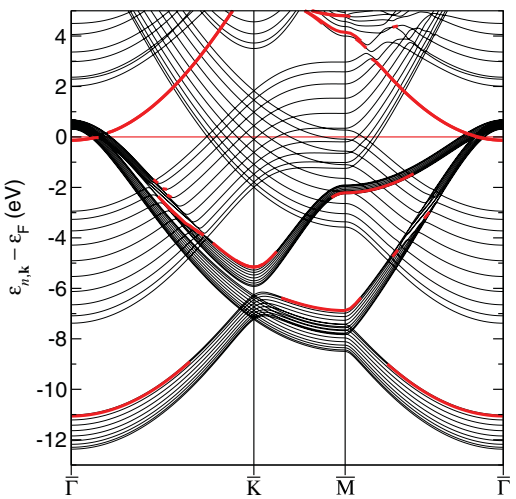

FIG. 10. (Color online) GPAW overlap-based band structure of relaxed Li terminated $MgB_2(0001)$ surface, with $\psi_{n,\mathbf{k}} \rightarrow \psi_{n',\mathbf{k}+\Delta\mathbf{k}}$ for n' which maximizes $|\langle\psi_{n,\mathbf{k}}|\psi_{n',\mathbf{k}+\Delta\mathbf{k}}\rangle_\nu|$. Surface states with more than two thirds of their weight in the first vacuum and first two bulk layers, $s_{n,\mathbf{k}} \gtrsim 0.66$, are shown separately as thicker lines.

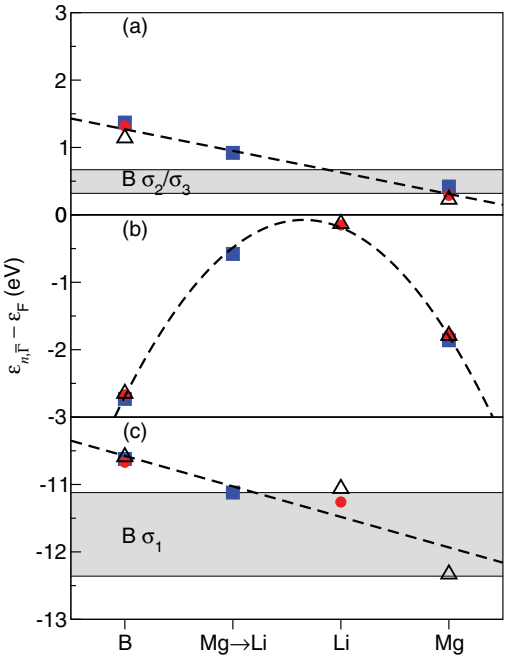

FIG. 11. (Color online) Surface and subsurface state energies at the $\bar{\Gamma}$ point, $\varepsilon_{n,\bar{\Gamma}}$ vs surface termination and doping of the $MgB_2(0001)$ surface by B, Mg→Li∼Mg^{+1}, Li, and Mg, in eV relative to the Fermi level ε_F, for (a) B σ_2 and σ_3, (b) sp_z, and (c) B σ_1 states. Results from plane wave PWscf calculations before (■) and after (●) structural optimization are compared with real-space GPAW calculations for the relaxed structures (△). The B $\sigma_{2,3}$ and B σ_1 bulk band regions are shaded gray. Fits to the surface state positions (– –) are provided as guides to the eye.

but are "free" to move within the band. In this way, the B σ surface bands may be considered a 2D electron gas decoupled from the surrounding 3D electron gas of the bulk MgB_2. Such a two-component electron plasma allows different types of plasma dispersion relations in the low-energy domain in addition to a conventional surface plasmon[34] which was described in MgB_2 recently.[24,25] For example, an acoustic surface plasmon[35] may be present, whose dispersion resembles that of the acoustic phonons with the slope determined by the Fermi velocity of a surface state.[35] This plasmon has been observed on a variety of metal surfaces[36–38] as well as in graphene layers adsorbed on different metal substrates.[39–42] Due to its sound-like dispersion, such a plasmon may affect (screen) the electron-phonon coupling.[22,43] Indeed, the MgB_2 surfaces present a quite unique situation for the realization of several acoustic surface plasmons with several surface bands crossing the Fermi level with Fermi velocities listed in Table V. Moreover, one may expect an anisotropy in their dispersion up to ∼50% due to the anisotropy in the surface state Fermi velocities seen in Table V.

On the other hand, for the sp_z state shown in Fig. 11(b), the energy of the surface state does not correlate with charging of the B atomic layer. Instead, to understand the behavior of the sp_z state, we must first consider its projected density $\varrho_{n,\bar{\Gamma}}(z)$. For each termination we find that the sp_z state is an ionic/metallic bonding state between the Mg/Li and B atomic layers. This is clear from Figs. 2(d), 5(a), and 8(d), where we

TABLE V. Fermi velocities v_F in atomic units of the σ_2, σ_3, and sp_z surface states for B, Mg, and Li terminations of the $MgB_2(0001)$ surface in the $\overline{\Gamma} \rightarrow \overline{K}$ and $\overline{\Gamma} \rightarrow \overline{M}$ directions.

	$\overline{\Gamma} \rightarrow \overline{K}$			$\overline{\Gamma} \rightarrow \overline{M}$		
Termination	$v_F^{\sigma_2}$	$v_F^{\sigma_3}$	$v_F^{sp_z}$	$v_F^{\sigma_2}$	$v_F^{\sigma_3}$	$v_F^{sp_z}$
B	0.42	0.34	0.36	0.46	0.22	0.32
Mg	0.26	0.20	0.34	0.27	0.18	0.33
Li	—	—	0.1	—	—	0.11

see that the sp_z state has mostly p_z character localized in the interlayer region. Specifically, for B termination the sp_z has significant weight in the bulk, while for Mg and Li terminations the sp_z state has more s character, with significant weight in the vacuum region.

This is also clear from the band structures shown in Figs. 4, 7, and 10. Specifically, for B termination (cf. Fig. 4) the sp_z state is at the top of the broad π band, having mostly p_z character, and is filled throughout most of the SBZ. For the Mg terminated surface (cf. Fig. 7) the sp_z state has more s character, is separated from the bulk π bands although still following the π bands through the SBZ, is shifted up in energy, and partially emptied. When we directly replace Mg by Li to model a Mg^{+1} surface, we find that the sp_z surface state has mostly Mg/Li s character [cf. Fig. 8(d)], is shifted up in energy between the π and Mg s bulk states, and is almost completely empty. For the relaxed Li terminated surface (cf. Fig. 10) the sp_z state is nearly emptied, and has significant s character, as shown in Fig. 8(d).

Together, this suggests that by altering the termination of the $MgB_2(0001)$ surface, the sp_z surface state is changed from a bulk-like state with p_z character for B termination, to an increasingly localized and emptied surface state with more metallic s character from Mg termination, to Mg→Li (or Mg^{+1}) termination, and finally the structurally optimized Li termination. This is consistent with previous calculations for the Na terminated $MgB_2(0001)$ surface,[13] which found the sp_z surface state between that calculated here for Mg and Mg→Li terminations. In effect, by varying the surface termination or electrochemically doping the surface, one can tune both the localization and energy range of $MgB_2(0001)$ sp_z surface states.

In this way, one could then modify the density or Fermi velocity of the charge carriers on the surface and consequently low-energy surface plasmon dispersions.[35] This means that surface plasmon characteristics may be tuned rather easily by surface charging or doping.

V. CONCLUSIONS

In this paper we have investigated $MgB_2(0001)$ surface and subsurface states, and the influence of surface termination (by B, Mg, and Li) and surface charging (replacing Mg by Li to model Mg^{+1}) using both plane wave and real-space *ab initio* methods. Generally we find for the $MgB_2(0001)$ surface there exist three types of surface states which are often well separated from bulk bands, namely, the B σ_1 surface band, the sp_z suprasurface state band, and the B σ_2 and σ_3 QW bands.

If charge is added to the B layer by either changing the surface termination or surface charging, the B σ surface bands shift down in energy. As these bands cross the bulk B σ bands, they lose their surface state character due to hybridization. In effect, by adjusting the charging of the B subsurface atomic layer, we may tune both the localization and energy range of the B σ surface states.

On the other hand, the addition of a Mg, Mg^{+1}, or Li layer above the B surface layer gives the sp_z surface state band an increasingly metallic s character as it is emptied. We find these results are quite robust, and independent of the *ab initio* methodology employed (plane wave or real-space) and relaxation of the surface.

Overall, these results suggest that by changing surface coverage and charging, one may tune both the density and Fermi velocity of the charge carriers at the surface. This would make possible the controlled modification of the surface plasmon dispersions, for example, the slope of the acoustic surface plasmons, which may then influence (modify or enhance) "surface" superconductivity. This has profound implications for both the superconducting behavior and low-energy surface or acoustic surface plasmon dispersion of MgB_2.

Therefore, because of the diversity of MgB_2's surface electronic structure, with combinations of various types of quasi-2D and 3D plasmas, it seems that the MgB_2 surface should have very unusual dielectric and optical properties. To clarify these unique properties, our next step will be the investigation of the MgB_2 surface dielectric response.

ACKNOWLEDGMENTS

We acknowledge funding through the Spanish "Juan de la Cierva" program (JCI-2010-08156), Spanish Ministerio de Ciencia e Innovacíon (FIS2010-21282-C02-01, FIS2010-19609-C02-01), Spanish "Grupos Consolidados UPV/EHU del Gobierno Vasco" (IT-319-07, IT-366-07), and ACI-Promociona (ACI2009-1036). The European Theoretical Spectroscopy Facility is funded through ETSF-I3 (Contract No. 211956).

*vito@phy.hr

[1] J. Nagamatsu, N. Nakagawa, T. Muranaka, Y. Zenitani, and J. Akimitsu, Nature (London) **410**, 63 (2001).
[2] S. Souma *et al.*, Nature (London) **423**, 65 (2003).
[3] Y. Zhang, Z. Lin, Q. Dai, D. Li, Y. Wang, Y. Zhang, Y. Wang, and Q. Feng, Supercond. Sci. Technol. **24**, 015013 (2011).
[4] K. D. Belashchenko, M. van Schilfgaarde, and V. P. Antropov, Phys. Rev. B **64**, 092503 (2001).
[5] J. Kortus, I. I. Mazin, K. D. Belashchenko, V. P. Antropov, and L. L. Boyer, Phys. Rev. Lett. **86**, 4656 (2001).
[6] I. I. Mazin and V. P. Antropov, Physica C **385**, 49 (2003).
[7] J. M. An and W. E. Pickett, Phys. Rev. Lett. **86**, 4366 (2001).
[8] I. T. Belash, A. D. Bronnikov, O. V. Zharikov, and A. V. Palnichenko, Solid State Commun. **64**, 1445 (1987).
[9] I. G. Kim, J. I. Lee, B. I. Min, and A. J. Freeman, Phys. Rev. B **64**, 020508(R) (2001).

[10]Z. Li, J. Yang, J. G. Hou, and Q. Zhu, Phys. Rev. B **65**, 100507(R) (2002).
[11]V. M. Silkin, E. V. Chulkov, and P. M. Echenique, Phys. Rev. B **64**, 172512 (2001).
[12]V. D. P. Servedio, S. L. Drechsler, and T. Mishonov, Phys. Rev. B **66**, 140502(R) (2002).
[13]G. Profeta, A. Continenza, F. Bernardini, and S. Massidda, Phys. Rev. B **66**, 184517 (2002).
[14]H. Uchiyama, K. M. Shen, S. Lee, A. Damascelli, D. H. Lu, D. L. Feng, Z.-X. Shen, and S. Tajima, Phys. Rev. Lett. **88**, 157002 (2002).
[15]C. Cepek, R. Macovez, M. Sancrotti, L. Petaccia, R. Larciprete, S. Lizzit, and A. Goldoni, Appl. Phys. Lett. **85**, 976 (2004).
[16]R. Macovez, C. Cepek, M. Sancrotti, A. Goldoni, L. Petaccia, R. Larciprete, and S. Lizzit, J. Phys. Condens. Matter **16**, 3451 (2004).
[17]L. Petaccia, C. Cepek, S. Lizzit, R. Larciprete, R. Macovez, M. Sancrotti, and A. Goldoni, New J. Phys. **8**, 12 (2006).
[18]V. P. Zhukov, V. M. Silkin, E. V. Chulkov, and P. M. Echenique, Phys. Rev. B **64**, 180507 (2001).
[19]W. Ku, W. E. Pickett, R. T. Scalettar, and A. G. Eguiluz, Phys. Rev. Lett. **88**, 057001 (2002).
[20]Y. Q. Cai *et al.*, Phys. Rev. Lett. **97**, 176402 (2006).
[21]A. Balassis, E. V. Chulkov, P. M. Echenique, and V. M. Silkin, Phys. Rev. B **78**, 224502 (2008).
[22]V. M. Silkin, A. Balassis, P. M. Echenique, and E. V. Chulkov, Phys. Rev. B **80**, 054521 (2009).
[23]V. Guritanu, A. B. Kuzmenko, D. van der Marel, S. M. Kazakov, N. D. Zhigadlo, and J. Karpinski, Phys. Rev. B **73**, 104509 (2006).
[24]A.-G. Kussow, A. Akyurtlu, A. Semichaevsky, and N. Angkawisittpan, Phys. Rev. B **76**, 195123 (2007).
[25]N. Limberopoulos, A. Akyurtlu, K. Higginson, A.-G. Kussow, and C. D. Merritt, Appl. Phys. Lett. **95**, 023306 (2009).
[26]P. Giannozzi *et al.*, J. Phys. Condens. Matter **21**, 395502 (2009).
[27]J. J. Mortensen, L. B. Hansen, and K. W. Jacobsen, Phys. Rev. B **71**, 035109 (2005).
[28]J. Enkovaara *et al.*, J. Phys. Condens. Matter **22**, 253202 (2010).
[29]J. P. Perdew and A. Zunger, Phys. Rev. B **23**, 5048 (1981).
[30]N. Troullier and J. L. Martins, Phys. Rev. B **43**, 1993 (1991).
[31]C. Kittel, *Introduction to Solid State Physics*, 7th ed. (John Wiley, New York, 1996).
[32]D. J. Mowbray, J. I. Martínez, F. Calle-Vallejo, J. Rossmeisl, K. S. Thygesen, K. W. Jacobsen, and J. K. Nørskov, J. Phys. Chem. C **115**, 2244 (2011).
[33]J. P. Perdew, K. Burke, and M. Ernzerhof, Phys. Rev. Lett. **77**, 3865 (1996).
[34]R. H. Ritchie, Phys. Rev. **106**, 874 (1957).
[35]V. M. Silkin, A. García-Lekue, J. M. Pitarke, E. V. Chulkov, E. Zaremba, and P. M. Echenique, Europhys. Lett. **66**, 260 (2004).
[36]B. Diaconescu, K. Pohl, L. Vattuone, L. Savio, Ph. Hofmann, V. M. Silkin, J. M. Pitarke, E. V. Chulkov, P. M. Echenique, D. Farías, and M. Rocca, Nature (London) **448**, 57 (2007).
[37]S. J. Park and R. E. Palmer, Phys. Rev. Lett. **105**, 016801 (2010).
[38]K. Pohl, B. Diaconescu, G. Vercelli, L. Vattuone, V. M. Silkin, E. V. Chulkov, P. M. Echenique, and M. Rocca, Europhys. Lett. **90**, 57006 (2010).
[39]Y. Liu and R. F. Willis, Phys. Rev. B **81**, 081406 (2010).
[40]H. Pfnür, T. Langer, J. Baringhaus, and C. Tegenkamp, J. Phys. Condens. Matter **23**, 112204 (2011).
[41]T. Langer, D. F. Förster, C. Busse, T. Michely, H. Pfnür, and C. Tegenkamp, New J. Phys. **13**, 053006 (2011).
[42]A. Politano, A. R. Marino, V. Formoso, D. Farías, R. Miranda, and G. Chiarello, Phys. Rev. B **84**, 033401 (2011).
[43]E. H. Hwang, R. Sensarma, and S. Das Sarma, Phys. Rev. B **82**, 195406 (2010).